Mass spectrometry-based phospholipid imaging: methods and findings

Review Article

Mass spectrometry-based phospholipid imaging: methods and findings

Md. Al Mamun[1], Ariful Islam[1], Fumihiro Eto[1], Tomohito Sato[1], Tomoaki Kahyo[1], Mitsutoshi Setou[1,2,3,*]

[1]Department of Cellular & Molecular Anatomy, Hamamatsu University School of Medicine, 1-20-1 Handayama, Higashi-ku, Hamamatsu, Shizuoka 431-3192, Japan.

[2]International Mass Imaging Center, Hamamatsu University School of Medicine, 1-20-1 Handayama, Higashi-ku, Hamamatsu, Shizuoka 431-3192, Japan.

[3]Department of Systems Molecular Anatomy, Institute for Medical Photonics Research, Preeminent Medical Photonics Education & Research Center, 1-20-1 Handayama, Higashi-ku, Hamamatsu, Shizuoka 431-3192, Japan.

*Correspondence: setou@hama-med.ac.jp; Tel.: 053-435-2086; Fax: 053-435-2468

Abstract

Introduction: Imaging is a technique used for direct visualization of the internal structure or distribution of biomolecules of a living system in a two-dimensional or three-dimensional fashion. Phospholipids are important structural components of biological membranes and have been reported to be associated with various human diseases. Therefore, the visualization of phospholipids is crucial to understand the underlying mechanism of cellular and molecular processes in normal and diseased conditions.

Areas covered: Mass spectrometry imaging (MSI) has enabled the label-free imaging of individual phospholipids in biological tissues and cells. The commonly used MSI techniques include matrix-assisted laser desorption ionization-MSI (MALDI-MSI), desorption electrospray ionization-MSI (DESI-MSI), and secondary ion mass spectrometry (SIMS) imaging. This special report described those methods, summarized the findings, and discussed the future development for the imaging of phospholipids.

Expert opinion: Phospholipids imaging in complex biological samples has been significantly benefited from the development of MSI methods. In MALDI-MSI, novel matrix that produces homogenous crystals exclusively with polar lipids is important for phospholipids imaging with greater efficiency and higher spatial resolution. DESI-MSI has the potential of live imaging of the biological surface while SIMS is expected to image at the subcellular level in the near future.

Keywords: Phospholipid; Mass spectrometry imaging; MALDI-MSI; DESI-MSI; SIMS imaging.

Highlights:

1. Mass spectrometry imaging (MSI) is a powerful method for imaging specific phospholipids (PLs) in tissues and cells.
2. The potential of MSI of either single or multiple PLs for the development of therapeutic agents, biomarkers, and predictive factors for diseases is reviewed.
3. The current states of MALDI-MSI, DESI-MSI, and SIMS-MSI on tissue PL imaging are assessed and discussed.
4. By image reconstruction, conventional 2D imaging can be applied in 3D PL imaging.

1. Introduction

In biology, imaging refers to the technique used to visualize the internal structure or biomolecules in tissues and cells of a living system in two- dimensional (2D) or three-dimensional (3D) style without perturbing the structure. The history of imaging dates back to 1895 when Wilhelm Roentgen discovered X-ray. X-ray was originally used in medical imaging to create 2D image of internal organs in an X-ray film [1]. With the advancement of computer vision and algorithms, several methods such as computed tomography [2], magnetic resonance imaging [3], positron emission tomography [4] and ultrasound [5] have been evolved to produce 2D as well as 3D image [6]. Besides anatomical imaging, those techniques play important role in molecular imaging where contrast agents are used for the noninvasive visualization, characterization, and measurement of the biological processes in the living system [6,7,8]. Discovery of electron microscope enabled the comprehensive visualization of cellular and subcellular ultrastructures [9]. Some other microscopy-based labelled molecular imaging techniques such as green fluorescent protein labelling [10], and immunohistochemistry [11] are used to visualize the distribution map of protein molecules in tissue as well as cell structure.

Phospholipids (PLs) are one of the major structural components of biological membranes [12,13] and play important roles in protecting the cells and organelles [14]. They also act as signaling molecules [15] and precursors of many signaling mediators for various biological processes [14,16]. An increasing amount of evidence indicates that the altered level of PLs and their metabolites in tissues are associated with various human diseases such as cancers [17], cardiovascular diseases [18], diabetes [19], Alzheimer's disease (AD) [20,21], and autoimmune inflammatory diseases [22]. Therefore, it is important to visualize individual PL species in tissue as well as in cellular level in order to explore the underlying mechanism of cellular and molecular processes in normal and diseased conditions. However, PLs in tissue sections cannot be imaged with conventional molecular imaging techniques. Some staining methods such as Nile red [23], Oil Red O [24,25] or osmium tetroxide [26] is commonly used to localize the PL fraction on frozen tissue sections. However, these methods localize either the complete lipid fraction or only one PL class on tissue sections, not individual PL species. Unlike immunohistochemistry of proteins, there is no such protocol for individual PL imaging due to the lack of antibodies or fluorescent probes.

Conventional mass spectrometry (MS) including liquid chromatography-MS (LC-MS) has been extensively employed in lipidomics, particularly in the identification and quantification of PLs in biological tissue [27,28]. Typical sample preparation protocol in LC-MS includes the homogenization of tissue sample followed by lipid extraction resulting in the loss of spatial information. LC-MS analysis of lipids extracted from various anatomical regions of a certain tissue such as the brain is often investigated in order to retain the spatial information [29,30]. However, it is a time-consuming process and cannot resolve the microscopic anatomical regions because of the challenges in the dissection and lipid extraction processes. In addition, the method requires a huge amount of sample that limits the analysis of important clinical samples such as biopsy tissues. Fortunately, MS has undergone tremendous development particularly in sample preparation protocol and instrumentation enabling the analysis of biomolecules directly from the thin tissue section to visualize individual molecule over the entire tissue [31,32].

So far, this method commonly known as imaging mass spectrometry (IMS) or mass spectrometry imaging (MSI) has revolutionized the comprehensive imaging (2D and 3D) of PLs in complex biological tissues. In this report, we focused on this technique in PLs imaging including the methodologies and findings.

2. Structure and classification of PL species

PLs are diverse in chemical structures consisting of a hydrophilic head group and one or more hydrophobic acyl chains attached to an alcohol moiety [14], and are commonly referred to glycerophospholipids (GPLs) [33]. GPLs are esters of glycerol, fatty acids, and phosphoric acid(s), where glycerol acts as the backbone. Two fatty acid chains are generally present at the sn-1 and sn-2 positions, whereas the phosphate group is linked to the sn-3 position of the glycerol backbone. The head group is attached to the phosphate group(s), and its chemical nature can be diverse, leading to different GPLs. The most common GPLs containing a single phosphate group are phosphatidylcholine (PC), phosphatidylethanolamine (PE), phosphatidylinositol (PI), phosphatidylserine (PS), phosphatidylglycerol (PG) and phosphatidic acid (PA). A subclass of GPLs is the lysophospholipids (LPLs), in which a single fatty acid is present at either sn-1 or sn-2 position of the glycerol backbone. Examples of LPLs include lysophosphatidic acid (LPA), lysophosphatidylcholine (LPC), lysophosphatidylethanolamine (LPE), lysophosphatidylinositol (LPI), lysophosphatidylglycerol (LPG), and lysophosphatidylserine (LPS). Diphosphatidylglycerol, historically known as cardiolipin (CL), is a unique mitochondrial PL that contains two phosphate groups and four acyl chains linked to the glycerol backbone (Table 1).

Various combinations of fatty acids and head group to the alcohol backbone, and their oxidation products resulted in the remarkable structural diversity (Table 1) and biological functions of the PLs molecules.

Table 1: Names and structures of major phospholipids occurring in the living system.

Major phospholipids	General structure
Phosphatidylcholine	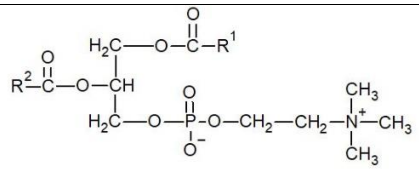
Phosphatidylethanolamine	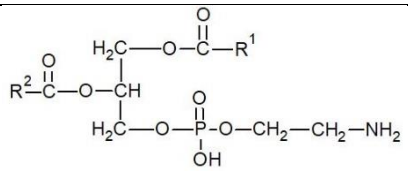
Phosphatidylserine	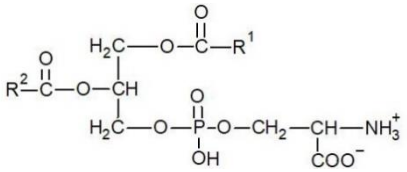
Phosphatidylinositol	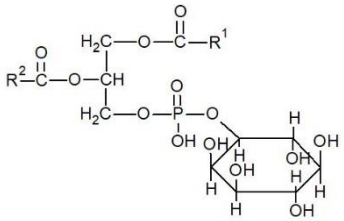
Phosphatidylglycerol	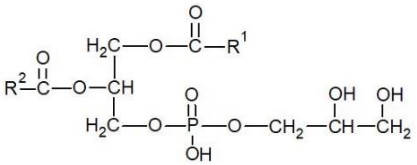
Phosphatidic acid	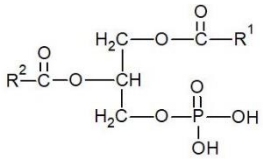
Cardiolipin	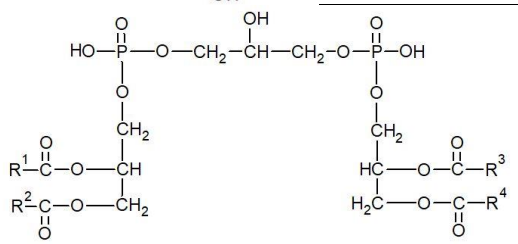

N.B.: R^1, R^2, R^3 and R^4 indicate acyl chains of fatty acids.

3. Methods of PLs imaging by MSI

MSI is a powerful technique that allows the simultaneous imaging of hundreds of biomolecules in thin tissue sections without extraction, purification or separation [34]. It is a label-free molecular imaging method which was initially used to map proteins and peptides in biological tissues [35]. In the last several years, this technique has been utilized extensively in the visualization of individual PLs in a variety of human and animal samples [36].

3.1 Instrumentation for MSI

Like conventional MS, the basic instrumentation of MSI includes (i) an ionization source to generate ions from neutral molecules, (ii) a mass analyzer to analyze ions based on the mass-to-charge ratio (*m/z*), and (iii) a detector to subsequently detect the ions and convert into digital signals. The fundamental difference with the conventional MS is that it collects ions directly from the surface area of a sample under controlled motion resulting in the preservation of the spatial information.

Numerous ionization sources originally developed for MS have been utilized further for MSI analysis. Among the various ionization sources used for MSI, matrix-assisted laser desorption ionization-MSI (MALDI-MSI) [37], desorption electrospray ionization-MSI (DESI-MSI) [38], and secondary ion mass spectrometry (SIMS) imaging [39] are most prominent. Several variants of MALDI-MSI include infrared-matrix-assisted laser desorption electrospray ionization (IR-MALDESI) [40,41], atmospheric pressure scanning microprobe MALDI (AP-SMALDI) [42], atmospheric pressure-MALDI-MSI (AP-MALDI-MSI) [43], and matrix-free laser desorption ionization (LDI) techniques such as nano-assisted laser desorption ionization-MSI (NALDI-MSI) [44] and desorption ionization using through-hole alumina membrane-MSI (DIUTHAME-MSI) [45]. Some other techniques such as laser ablation electrospray ionization (LAESI) [46], air flow-assisted ionization-MSI (AFAI-MSI) [47], and easy ambient sonic spray ionization (EASI) [48], have also been developed for imaging. The current report mainly focused on the three major ionization techniques namely MALDI, DESI, and SIMS for PLs imaging.

A variety of mass analyzers compatible with ionization sources are available for MSI analysis. Time-of-flight (TOF) is the most common mass analyzer used for MSI due to their high mass range, sensitivity and fragmentation capabilities in tandem MS. Ion trap and quadrupole time-of-flight (QTOF) are also widely used in MALDI-MSI and DESI-MSI. The use of Fourier-transform ion cyclotron resonance (FT-ICR) mass analyzer in MALDI-MSI has significantly increased the molecular imaging with high mass resolution. Each analyzer separates ions in a physically distinct mechanism, and has specific advantages and limitations.

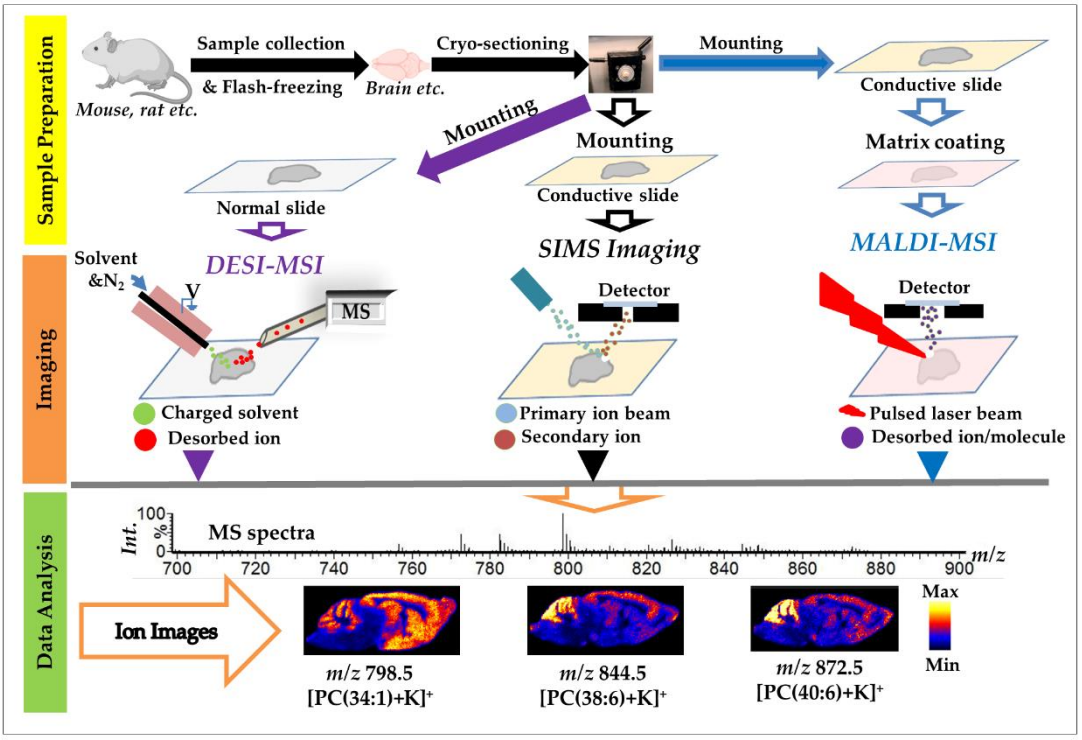

Figure 1: Overview of phospholipid imaging by mass spectrometry imaging. Tissue samples collected from human or animal sources are flash-frozen, cryosectioned, and thaw-mounted on a glass slide. For MALDI-MSI and SIMS imaging, the tissue section is generally mounted on indium tin oxide (ITO)-coated glass slide whereas DESI-MSI uses normal glass slide. Unlike MALDI-MSI, SIMS imaging and DESI-MSI do not require matrix-coating. The sample is placed onto a 2D moving stage and subjected to ionization usually in a raster fashion as the sample stage moves in x, y coordinates at a controlled speed. The ions are then analyzed based on the mass-to-charge ratio (*m/z*) in a mass analyzer. A detector subsequently detects those ions and converts them into digital signals. Results are displayed as mass spectra as well as two-dimensional ion-images. The mass spectra and the ion images shown here were acquired by DESI-MSI of mice brain sections.

3.2 Sample preparation for MSI

In MSI of PLs, careful sample preparation is crucial for successful imaging as the polyunsaturated fatty acid containing-PLs (PUFA-PLs) are prone to oxidization.

3.2.1 Tissue sample preparation

Collection of samples – The use of thin sections of human and animal (usually mice and rats) tissues is very common in PLs imaging. Human samples used for imaging include the biopsy and the archived post-mortem tissues. Animals are usually euthanized by cervical dislocation or using anesthetics prior to tissue collection. In order to preserve the tissue anatomy and to halt the enzymatic degradation, tissues should be dissected rapidly

followed by immediate flash-freezing using powdered-dry ice or liquid nitrogen (Figure 1). The frozen tissues are then stored at -80 °C until sectioning.

Cryo-sectioning– Before slicing, frozen tissues are transferred into a cryostat chamber and left for 15 – 20 minutes at – 10 °C to – 20 °C to equilibrate to the sectioning temperature. Tissue block is affixed to the stage of a cryostat machine using an embedding media and then sliced at a thickness of around 5 – 20 µm. For 3D MSI, a series of serial sections are collected with minimal error and registered carefully. During sectioning, optimized temperature, usually at – 20 °C (can vary depending on the type of tissue), must be maintained in the cryostat. Particular care should be taken when using optimal cutting temperature embedding media (OCT) or other embedding media containing polymer as they cause serious contamination reducing the quality of the spectra. The thickness of the section should be as thin as possible to achieve higher quality spectral data in MALDI-MSI [49], although DESI-MSI has the flexibility regarding the sample thickness.

Sample pre-treatment – For MALDI, the tissue section is generally thaw-mounted on an indium tin oxide (ITO)-coated glass slide followed by a homogenous coating with a suitable matrix solution allowing the formation of co-crystals between the matrix molecules and the analytes. The matrix molecules must have the property of absorbing laser energy to aid in the ionization process. Various matrix compounds have been developed due to the fact that a single matrix does not work for all PLs. For instance, 2,5-Dihydroxybenzoic acid is commonly used to image PC molecules [50,51] in positive ion mode while 9-aminoacridine is used for imaging various PLs including PI, PG, PS, PA and CL in negative ion mode [52]. Other matrices that have been used for the imaging of PLs include 2,5-dihydroxyacetophenone [53], α-cyano-4-hydroxycinnamic acid [50], graphene oxide [54], and 1,6-Diphenyl-1,3,5-hexatriene [55]. The matrix can be sprayed either manually (e.g., using artistic air brush) or automatically (e.g., using TM-Sprayer™ manufactured by HTX Technologies, and ImagePrep manufactured by Bruker Daltonics Inc.) [56].

Unlike MALDI, DESI uses normal glass slide for tissue mounting and does not require sample pre-treatment reducing the time significantly for sample preparation.

For SIMS imaging, the tissue section is generally transferred onto the ITO-coated glass slide and does not require matrix coating. Unfortunately, the high energy primary ion beam used in typical SIMS causes increased fragmentation of the PLs resulting in the poor molecular ion yield. In order to reduce the fragmentations, several approaches for sample preparation such as matrix enhancement (similar to MALDI protocol) and surface metallization (coating with a thin layer of gold or silver) have been developed [57].

3.2.2 Sample preparation for single-cell imaging

PLs imaging at the cellular level has been made possible by SIMS imaging as it offers the capability of resolving very small features which can be as low as a hundred nanometers. Sample for single-cell analysis includes the isolated cells from the specimen or cultured cell. Unfortunately, live cells cannot be analyzed directly in SIMS as it works under a high vacuum condition. Generally, cells are extracted or grown on an appropriate substrate such as silicon wafer or gold-coated silicon wafer [58] followed by fixation to minimize sample degradation. Two fixation methods are commonly applied: (i) chemical fixation using glutaraldehyde, and (ii) cryofixation. A cryofixation method, namely

plunge fixation, has been shown to be advantageous for single-cell lipid imaging [59]. In plunge freezing, samples are stored in liquid nitrogen at -196 °C after washing by a mixture of propane and isopentane (3:1). Interestingly, enhanced signal intensity for PLs has been reported when matrix solution is added on the cell surface prior to the fixation [58]. After fixation, frozen samples are freeze-dried and stored until analysis.

3.3 Analysis by MSI

To minimize the degradation or oxidation of the PLs, imaging should be performed as soon as possible once the sample is ready for analysis. The sample is placed onto a 2D moving stage and subjected to ionization either in positive or negative ion mode. Ions are collected from the surface usually in a raster fashion as the sample stage moves in x, y coordinates at a controlled speed. The ions are then sent into the mass analyzer for analysis and subsequently detected by the detector system.

PLs are a large group of molecules and show diversity in ion production. PC and PE are typically ionized in positive ion mode as protonated/sodiated/potassiated adducts while PS, PA, PI, and PG are ionized in negative ion mode as deprotonated ions in the mass range of *m/z* 700 – 900. LPLs are detected either in positive or negative ion mode in the mass range of *m/z* 400 – 600, on the other hand, singly charged CLs are usually detected in the negative ion mode in the mass range of *m/z* 1000 – 1600.

MALDI is a widely used soft ionization process that primarily produces singly-charged ions in both positive and negative ion modes. In this method, the matrix-coated sample surface is irradiated by pulsed laser causing the rapid excitation and heating of the matrix molecules [60,61] (Figure 1). The heated molecules undergo evaporation resulting in the desorption of neutral and charged analytes, matrix molecules, analyte-matrix, and matrix-matrix clusters, all under the vacuum conditions. Ionization of the analytes are thought to occur during the desorption process, or in the expanding plume through the charge transfer between the excited matrix molecules and the neutral analytes. Ultraviolet lasers such as frequency-tripled Nd:YAG lasers (355 nm) are commonly used for MALDI-MSI as they are strongly absorbed by the matrix molecules [62].

Unlike MALDI, DESI works in an open environment at atmospheric pressure. In DESI, a beam of charged microdroplets of solvent coupled with a nebulizer nitrogen gas is directed continuously onto the tissue surface where molecules are extracted, ionized and desorbed into the mass spectrometer for analysis [63] (Figure 1). Methanol (usually 98%) is commonly sprayed at a flow rate of 2 —5 µL/min using a solvent pump, and a capillary voltage of 2 — 4.0 kV is generally applied to charge the solvent. A 2-D stage moves the tissue at a controlled speed to record the mass spectra from different spatial coordinates. The spatial resolution of DESI is lower (can range between 50—200 µm) than that of MALDI (typically <50 µm). However, nano-DESI can offer much higher spatial resolution (better than 10 µm) [64,65,66]. Prior to the analysis, optimization of several parameters such as solvent composition, solvent flow rate, gas flow rate, capillary voltage, cone voltage, inlet temperature, and the geometry of the sprayer is required in order to obtain the highest desorption and ionization as well as the best spatial resolution of the ion image [67,68].

Conventionally, SIMS uses a hard ionization technique where the tissue surface is bombarded with a focused high energy primary ion beam, causing desorption of

secondary ions into the mass analyzer. It operates either in dynamic or static modes, while the latter is used for PLs imaging as the intact molecular ions are typically detected under that condition. The emergence of cluster ion sources (e.g., C60+, Bi3+, and Au3+) as a primary ion beam has significantly improved the PLs imaging with high sensitivity [57]. Like MALDI, ionization events in SIMS occur under the vacuum conditions.

For single-cell analysis, freeze-dried cells are typically subjected to SIMS imaging. Interestingly, the increased signal intensity of PLs was observed when the sample is analyzed in frozen-hydrated conditions where the cryo-fixed cells are kept frozen with a liquid nitrogen-cooled stage during the analysis [69,57].

3.4 Data analysis

MSI data are multidimensional, and usually processed by in-built software visualizing as mass spectra (a plot of intensity vs. *m/z*), and 2D-ion images corresponding to each ion signal (Figure 1). In 3D MSI, suitable 2D ion images acquired from a series of serial sections are combined to construct a 3D image. Each pixel of the ion image contains a mass spectrum of all molecules detected at that irradiated/sprayed area. Data normalization to the total ion current is often used to eliminate artifacts. MSI has the strength of combining (e.g., overlay, merge etc.) an ion image corresponding to a certain signal with the microscopic data (e.g. H&E stained image) of the same or serial tissue section allowing the interpretation of the spatial distribution within the histological context. Mass spectra from different regions of interest (ROIs) of an ion image can be extracted and compared. Multivariate analysis methods (MVA), particularly, principal component analysis (unsupervised method) and partial least-squares regression (supervised method) are widely used to classify or differentiate between ROIs or samples by reducing the dimensionality of the MSI data. MVA is often used in combination with discriminant analysis to examine how well the ROIs or samples are differentiated. Statistical analyses such as t-tests and ANOVA are performed to evaluate whether the observed distributional changes are significant. For biomarker discovery, a receiver operator characteristic curve analysis is often performed that calculates the sensitivity and specificity of individual ions.

Unambiguous molecular assignment to an *m/z* of interest is an important task in MSI. A careful assignment is highly recommended since an *m/z* value often presents a number of different molecular ions. In addition, two or more PLs can be detected at a single *m/z* value in the spectra as PLs show diversity in their head group, acyl chain moieties, and adduct forms. The tentative assignments of PLs are performed by matching the observed *m/z* value in the mass spectra to the reported literature or database of known compounds within an acceptable mass error range (typically 1-20 ppm, varies with the mass resolution of the analyzer). Several online databases such as human metabolome database (https://hmdb.ca/) [70], and lipid map (https://www.lipidmaps.org/) [71] are dedicated for this purpose. For unambiguous assignments, tandem mass spectrometry analysis (e.g., on-tissue MS/MS, LC-MS/MS of lipid extracts) is routinely performed where individual lipid species yield characteristic fragment ions (e.g., fragments specific to the head groups, sn-1 and sn-2 fatty acyl groups etc.) [72]. The fragmentation patterns of the ion of interest are compared with those of a pure compound analyzed under the identical conditions. Immunohistochemical analyses of protein(s) related to the PL of interest are often performed for further confirmations of the specific PL assignment [73,74].

4. Reports on PLs imaging by MSI

MSI has been employed extensively to explore the spatial distribution of PL species in a variety of biological samples [75]. MALDI-MSI is the most widely used techniques for PLs imaging followed by the DESI-MSI and SIMS imaging. By far the most detected PL species are the PCs while the most imaged tissues are brain and tumors.

4.1 MSI revealed the region-specific distributions of individual PLs

Distribution of specific PLs in different normal anatomical locations of biological tissues has been extensively studied. MALDI-MSI allowed visualizing the cell-selective distribution of polyunsaturated fatty acid-containing PCs (PUFA-PCs) in mouse brain: arachidonic acid-containing PCs and DHA-PCs were distributed in the hippocampal neurons and cerebellar Purkinje cells, respectively [76]. Two PLs, PI(38:4) and PC(36:1) were preferentially localized to the gray matter while PC(32:0) were preferentially localized to the white matter of rat brain [51]. PLs imaging in the human term placenta showed the differential distribution of PC(16:0_20:4) between the stem and terminal villi [77]. Two PC molecules, PC(16:0_18:2) and PC(16:0_18:1) were detected as the dominant molecules in the human gastric mucosa near the fundic glands [78]. DESI-MSI was capable of imaging 1-O-alkyl phosphatidylethanolamines and phosphatidylserines, PE (18:1e/18:1), and PS (18:1e/18:1) in a thin ring in the outermost region of the human lens [79]. Some other MALDI-MSI studies showed the distributions of PLs in various biological tissues including rat brain [80,81,82], heart [83], liver [84], mouse kidney [85], lung [86] and human lens [87]. ToF-SIMS imaging revealed the distribution of some specific PLs in the sections of the mouse brain [88], rat brain [89] and human skeletal muscle [90]. While the most imaged samples in the literature are tissues, several studies applied MALDI-MSI to profile PLs distribution in the whole body of some species including *Caenorhabditis elegans* [91], and *Drosophila melanogaster* [92].

4.2 PLs imaging determined the margin of diseased tissue

MSI has successfully revealed the altered distribution of some specific PLs in several diseased tissues thereby discriminating between diseased and healthy tissues [93,94]. This power of demarcation is of great help for the successful surgery of diseased tissue, particularly the tumors. In a MALDI-MSI study, our group reported that PC (36:1) was highly abundant in human breast cancer tissues than in the references [73] Margulis et al. used DESI-MSI and reported the distinct distribution of PG(18:1_16:0) and the relatively higher distribution of PS(18:1_18:0) and PI(18:0_20:4) in the human basal cell carcinoma tissue than in the normal skin [95]. Distinct distributions of PLs including PI(18:0/20:4) were seen in human seminoma and adjacent normal tissues [94]. In a study, 37 resected hepatocellular carcinoma tissues were analyzed by MALDI-MSI and revealed an increase of PC(16:0_16:1) and a decrease of LPC(16:0) in the cancerous region than in the normal region [96]. MALDI-MSI showed a higher accumulation of stearic acid and arachidonic acid-containing PI, PI(18:0_20:4), in the thickened wall than in the thinned wall of intracranial aneurysms [97]. Imaging of the ischemic rat brain revealed the production of LPC(16:0) in the area of focal cerebral ischemia [98].

4.3 PLs imaging showed the potentiality to the therapeutics discovery

A large number of MSI studies were performed to examine the changes of PLs level in tissues after a certain intervention in animal or insect, and thereby revealed the promising therapeutic agents for diseases. Recently, our group imaged PLs in the dorsal root ganglion (DRG) of mice after sciatic nerve transection (SNT) using MALDI-FTICR imaging at a spatial resolution of 25μM. The study showed that the arachidonic acid-containing PC (AA-PC), PC(16:0_20:4) highly increased while other two PCs and one PA(36:2) molecule decreased in the DRG following nerve transection [99]. LPA, an initiator of neuropathic pain, is generated from PA by phospholipase A2 enzymes [100] speculating that PA(36:2) is consumed to produce LPA [99]. Thus, the study suggested the potential use of LPA blocker for the treatment of neuropathic pain [99]. Our group employed MALDI-MSI and showed that a stearate and docosahexaenoic acid (DHA) containing PC (DHA-PC), PC(18:0_22:6), depleted in the grey matter of a post-mortem human AD brain [101] which was in excellent agreement with another study that revealed the improved memory function and distribution levels of brain DHA in senescence-accelerated mice P8 (SAMP8 mice), a model of dementia, supplemented with green nut oil (a rich source of α-linolenic acid) or DHA [102]. Recently, we used DESI-MSI technique to image the DHA-PCs in the brain of SAMP8 mice fed with green nut oil or DHA. SAMP8 mice brain showed the lower distribution of PC(16:0_22:6), and PC(18:0_22:6) compared to that of wild type mice. Interestingly, green nut oil or DHA treatment restored the decreased distribution of PC(16:0_22:6) and PC(18:0_22:6) in the brain of SAMP8 mice [72] suggesting the potential use of DHA and green nut oil in the prevention and treatment of dementia. Philipsen et al. examined the distribution of some individual phospholipids in Drosophila brain after the administration of cocaine and methylphenidate by ToF-SIMS imaging with a spatial resolution around 3 μM and revealed the possible involvement of brain lipids in learning and memory. Before treatment, two PCs, PC(34:1) and PC(34:2) were found to be abundant in the central brain while PE(34:1) and PI(36:4) were distributed throughout the brain. Cocaine administration largely changed the distribution of those PLs: PCs became more abundant in the central brain and optical lobe areas whereas the overall intensities of PE and PI decreased [103].

4.4 MSI identified PLs as a biomarker and predictive factor of diseases

MSI of PLs showed the promising power to the discovery of cancer biomarker and predictive factor of tumor recurrence which can potentially contribute to the improved disease management and monitoring of the disease progression. In a MALDI-MSI study, PC(16:0_16:1) was revealed as a novel biomarker in colorectal cancer [104]. PC (32:1) is highly abundant in recurrent triple-negative breast cancer (TNBC) tissues compared to the non-recurrent TNBC tissues making it as a potential predictive factor of TNBC recurrence [105]. High resolution-MALDI-MSI revealed the lower expression of LPC(16:0/OH) in prostate cancer than that in the benign prostate epithelium of human. These differences in expression of PLs will potentially help predict prostate cancer aggressiveness, and provide novel insights into the lipid metabolism in prostate cancer tissue [106]. In DESI-MSI study, lipids including several individual PCs, PGs and CLs were identified as biomarkers as well as predictive factors of serous ovarian cancer [93]. This methodology was utilized in classifying disease status, different subtypes and grades of several cancers including human bladder carcinomas [107], gliomas [108], renal cell carcinomas [109], and breast cancer [110]. Furthermore, Mao et al. showed the

application of AFAI-MSI in the rapid classification of human breast tumors based on the abundance of lipids including PLs [111].

4.5 Potential mechanism of cancer invasion revealed by PLs imaging

Membrane fluidity is thought to largely depend on the fatty acyl species linked to the PCs [112]. Compositional changes in the acyl chains may thus contribute to the altered fluidity influencing the behavior of the cancer cells, such as invasion and metastasis. Mapping of superficial-type pharyngeal carcinoma tissue sections from five human patients showed the higher distributions of three AA-PCs, PC(16:0_20:4), PC(18:1_20:4) and PC(18:0_20:4) in the subepithelial invasive region indicating the potential role of AA-PCs in the invasion mechanism [113].

4.6 CLs imaging

It is now clear that MSI has shown tremendous progress on PCs imaging in the last several years. PCs are the most abundant molecules in the membranes and also dominate the mass spectra due to their higher ionization efficiency than the other PL species. Unfortunately, these highly abundant molecules contribute to the ion suppression of some other PLs of low abundance. Due to this fact, the most reported PLs in the literature are the PCs, followed by LPLs and CLs.

CLs are unique mitochondrial PLs that play important structural as well as functional roles in bioenergetics and signaling [114]. They exist in a relatively small amount with remarkable diversification and are difficult to detect due to the ion suppressive effect of the highly abundant molecules present on the tissue surface. So far, a decrease level of CLs were reported in the kidney cortex of non-alcoholic steatohepatitis mice using the conventional MALDI-MSI protocol [115]. Several methods have been developed for CLs imaging by reducing or eliminating the ion suppressive effects. Amoscato et al. showed that the treatment of the tissue surface (prior to MALDI-MSI) with phospholipase C and 1-ethyl-3-[3-(dimethylamino)propyl]-carbodiimide hydrochloride (EDC) eliminates the ion suppressive effects by removing the highly abundant phosphatidylcholine head groups and cross-linking the accessible carboxyl/amino-containing molecules on the tissue, respectively [116]. Using this approach, authors successfully mapped multiple CLs and demonstrated a nonrandom distribution of PUFA and non-PUFA containing CLs in different anatomical locations of the male rat brain. Interestingly, the habenular nuclear/dorsal third ventricle and lateral ventricle areas of the brain showed a robust signal for CLs and were defined as the CL “hot spot” [116]. By employing similar methods, it was revealed that the traumatic brain injury in rats resulted in the early depletions in polyunsaturated CLs in the contusional cortex, ipsilateral hippocampus, and thalamus [117]. Recently, Yang et al. demonstrated an effective MALDI-MSI method for CLs mapping based on the sample preparation with norharmane matrix that does not require additional digestion procedure [118]. DESI-MSI showed the capability of direct CLs imaging in normal and cancer tissues. Several individual CLs with a smaller number of double bonds were shown to significantly increased in v-myc avian myelocytomatosis viral oncogene homolog (MYC)-induced lymphomas compared with normal tissue [119]. Furthermore, DESI-MSI identified cardiolipins as a molecular signature of mitochondria-rich thyroid oncocytic tumors [120].

4.7 Imaging of oxidized PLs

PUFA- containing PLs (PUFA-PLs) in the membrane undergoes oxidation by various enzymes or reactive oxygen species producing oxidized PLs. Oxidized PLs are highly bioactive molecules having both pro-inflammatory and anti-inflammatory effects and are now considered as markers of biological oxidative stress [121]. Oxidized PLs in human and animal tissues have been extensively studied by the LC-MS techniques [122]. Recently, there is a growing interest in imaging these modified PLs to discover biomarker for disease states and to advance the understanding of pathology. MALDI-MSI revealed a decrease of oxidizable PUFA-PLs including PS(18:0_22:6) in traumatic brain injury [75]. However, no reports on oxidized PLs imaging have been demonstrated using that method. So far, DESI-MSI identified several oxidized-CL species in mitochondria-rich thyroid oncocytic tumors [120].

4.8 Imaging of single-cell PLs

MALDI-MSI is capable of imaging at a spatial resolution less than 50 μM [99] and has been applied in PLs imaging at the cellular level. In a MALDI-MSI approach, flow cytometry-sorted single multiple myeloma cells and normal plasma cells were imaged with 5 μM laser ablation diameter and revealed a decrease of PC(16:0_20:4) in the malignant cells [123]. AP-MALDI imaging with 7 μM pixel size detected PC(32:1) and PC(34:1) primarily in the center of the HeLa cells where a large volume of membranes are expected [124]. However, these methods revealed only the gross PLs distribution on the cell surface.

So far, SIMS offers spatial resolution at a nanometer scale which is suitable for single-cell imaging. Unfortunately, PLs undergo severe fragmentations by the high energy primary ion beam resulting in the decreased spectral and image quality. Fragments of the phosphocholine head group are commonly seen in the mass spectra of SIMS, and they are often used to record the total PCs distribution. Ostrowski et al. employed TOF-SIMS under frozen-hydrated conditions to study the changes in the membrane lipid distribution during mating of *Tetrahymena thermophila* and observed a significant decrease of phosphocholine head group fragment along the conjugation junction [125].

Introduction of cluster ion sources and modifications in the sample preparation protocol have been developed discussed previously to reduce the fragmentations. Addition of matrix increased the signal intensity of several PCs including PC(34:1) on single-cell surface cultured on gold-coated silicon wafers [58]. Unfortunately, the crystals formed by matrix-coating mask some structural details on the cell surface, resulting in the poor image quality.

4.9 3D imaging of PLs

With the advancement of the image reconstruction method and the high-throughput analysis, MSI showed the ability to generate 3D images of PLs distribution in an entire organ or tissue. Patterson and coworkers developed a robust 3D MSI method using open-source software and revealed the distributions of LPC and PC molecules in human and mice carotid atherosclerosis tissues [126]. 3D MALDI-MSI technique has been applied to map PLs in newly fertilized zebrafish embryos: PCs were mostly distributed inside the yolk as well as in the blastodisc, while PEs and PIs were distributed minimally inside the yolk [127]. Paine et al. performed 3D MALDI-MSI on whole brains from a mouse model of human medulloblastoma and identified several PA, PE, PS, and PI molecules

associated with the metastasis [128]. DESI-MSI and SIMS imaging have also been utilized for 3D imaging of PLs in various tissues that include mice brain [129], glioblastoma xenograft [130], and Aedes aegypti ovarian follicles [131].

5. Conclusions

PLs imaging in complex biological tissues and cells has been revolutionized by the development of label-free MSI techniques. MALDI-MSI, DESI-MSI and SIMS imaging are the widely used MSI methods for the imaging of specific PLs, so far. MSI revealed the region-specific distributions of specific PLs in various tissues. Imaging of individual PLs demarcated the margins of cancers and contributed to the discovery of potential therapeutics, biomarkers, and predictive factors of diseases. Interestingly, the potential role of PLs in cancer invasion has been revealed by this technique. The abundance and the higher ionization efficiency of PCs contribute to the suppression of other PLS including CLs and oxidized PLs. Development in the sample preparation protocol enabled the successful imaging of CLs by reducing the ion suppression.

6. Expert opinion

MSI is a powerful method that has the capability of untargeted analysis of hundreds of molecules simultaneously in complex biological tissues and cells without labelling. These unique features made it a valuable tool for the visualization of proteins [132], lipids [36], nucleotides [133], neurotransmitters [134], small metabolites [135], and exogenous compounds [136] in a wide range of biological samples. It has become an indispensable tool for the imaging of individual PLs so far and greatly contributed to explore biomarkers as well as altered lipid distribution in various diseased states. However, there are many challenges in MSI of PLs exist.

Because of the variations of the acyl chains and the head groups, thousands of PL species could be present in a living cell. The head group attached to the phosphoric acid as well as the acyl chains of the glycerol backbone are detected and identified in tandem mass spectrometry. Unfortunately, the positional analysis of these chains (acyl chains specific to sn-1 and sn-2) is not possible in the current situation. In addition, on-tissue tandem MSI is often problematic due to the less sensitivity and the difficulty to isolate a target molecular ion from a myriad of molecules of the complex tissue sections. Therefore, imaging of PLs warrants further advancement of the mass analyzer for positional analysis of acyl chains and on-tissue MS/MS.

MSI is a surface analysis method and provides only the semi-quantitative information of the analytes. Although a lot of progress have been made in the development of methods, quantification is still one of the greatest challenges in MSI. A strategy for quantitative analysis could be the development of calibration curves using internal standards.

MALDI-MSI offers a better sensitivity for PLs detection than the other currently used MSI techniques. However, the choice of a matrix and the spray conditions directly affect the ionization efficiency and spatial resolution. A lot of efforts have been made to explore novel matrix and optimized spray conditions for successful imaging. Our group developed a two-step matrix application technique namely "spray-droplet method" that produce homogenous layer with minute crystals resulting in the improved ionization efficiency for MALDI-MSI [137]. Further development of matrix or alternative to the matrix that form homogenous crystals exclusively with polar lipids will potentially contribute to the PLs imaging with higher ionization efficiency and higher spatial resolution. The use of nanoparticle instead of matrix enabled the visualization of several PLs at an improved resolution (15 μm) in mammalian tissues [138].

DESI-MSI, a relatively new and nondestructive imaging method, has attracted much attention due to its capability of matrix-free simple analysis. In our experience, DESI-MSI is a suitable technique for analyzing small molecules [139,140,141] although it's spatial resolution and the ionization efficiency for PLs are lower than that of MALDI-MSI. DESI-MSI has a great potential of live imaging of biological surface molecules in clinical settings since it does not require any special sample preparation. Higher spatial resolution can be achieved through the advancement of the sprayer conditions (such as solvent flow rate, gas flow rate etc.) and the geometry of the ionization chamber while ionization efficiency for PLs can be improved by exploring the right solvent composition.

Nowadays, the need for PLs imaging at the sub-cellular level is increasing. Unlike tissue section imaging, single-cell imaging presents a great challenge as it requires techniques with high spatial resolution as well as high sensitivity because of the microscopic size and extremely small volume of analytes in a single cell. In DESI-MSI, pixel size is typically in the range of 50–200 μM, and thus single-cell structures cannot be resolved with this spatial resolution. Single-cell imaging by MALDI-MSI has revealed only the gross distributions of PLs. So far, SIMS has shown the capability of resolving features at the nanometer scale which allows for the imaging at the sub-cellular level. Unfortunately, it is difficult to detect PLs by this technique since fragmentation occurs during analysis. Some advancement including the use of cluster ion sources and the sample analysis under frozen-hydrated state significantly improved the PLs imaging.

Although MSI was primarily developed for 2D imaging, it has been applied for 3D imaging that significantly enhanced our understanding of the molecular processes. However, the current methodology for 3D MSI is laborious and time consuming. Interestingly, an automated 3D DESI-MSI method has been demonstrated for rapid analysis. In this technique, a robotic slide loader is installed to autonomously mount and change slides on the sample stage while the 2D ion images are automatically constructed and aligned to generate a 3D image [130].

Imaging of low abundance PLs including the CLs and oxidized PLs is still in its infancy. Methodological developments that reduce the ion suppression effect, and increase the sensitivity are warranted for the imaging of these molecules.

7. Acknowledgements

This work was supported by MEXT/JSPS KAKENHI (Grant Number JP15H05898B1), AMED (Grant Number JP20gm0910004), JSPS KAKENHI (Grant Number JP18H05268), and MEXT Project for promoting public utilization of advanced research infrastructure (Imaging Platform) under grant number JPMXS0410300220, Japan.

8. References

1. William G. Bradley. History of medical imaging. Proceedings of the American Philosophical Society. 152(3), 349–361(2008).
2. Kalender, W.A. X-ray computed tomography. Phys. Med. Biol. 51(13), R29-43(2006).
3. Grover, V.P.B.; Tognarelli, J.M.; Crossey, M.M.E.; Cox, I.J.; Taylor-Robinson, S.D.; McPhail, M.J.W. Magnetic resonance imaging: principles and techniques: lessons for clinicians. J. Clin. Exp. Hepatol. 5, 246–255 (2015).
4. Unterrainer, M.; Eze, C.; Ilhan, H., et al. Recent advances of PET imaging in clinical radiation oncology. Radiat. Oncol. 15, 1–15 (2020).
5. Seo, J.; Kim, Y. sun. Ultrasound imaging and beyond: recent advances in medical ultrasound. Biomed. Eng. Lett. 7, 57–58 (2017).
6. Pysz, M.A.; Gambhir, S.S.; Willmann, J.K. Molecular imaging: current status and emerging strategies. Clin. Radiol. 65, 500–516 (2010).
7. Deshpande, N.; Needles, A.; Willmann, J.K. Molecular ultrasound imaging: current status and future directions. Clin. Radiol. 65, 567–581 (2010).
8. Wu, M.; Shu, J. Multimodal Molecular Imaging: Current Status and Future Directions. Contrast Media Mol. Imaging. (2018).
9. Porter, K.R.; Claude, A.; Fullam, E.F. A study of tissue culture cells by electron microscopy: Methods and preliminary observations. J. Exp. Med. 81, 233–246 (1945).
10. Prendergast, F.G.; Mann, K.G. Chemical and physical properties of aequorin and the green fluorescent protein isolated from Aequorea forskålea. Biochemistry. 17, 3448–3453 (1978).
11. de Matos, L.L.; Trufelli, D.C.; de Matos, M.G.L.; Pinhal, M.A. da S. Immunohistochemistry as an important tool in biomarkers detection and clinical practice. Biomark. Insights. 5, 9–20 (2010).
12. Cevc, G. Phospholipids Handbook; CRC Press, 2018;
13. Chapman, D. Phospholipid bilayers physical principles and models. Cell Biochem. Funct. 6, 147–148 (1988).
14. Cai, T.; Yang, F. Phospholipid and Phospholipidomics in Health and Diseases. In; Springer, Singapore, pp. 177–202 (2018).

15. Birge, R.B.; Boeltz, S.; Kumar, S.; et al. Phosphatidylserine is a global immunosuppressive signal in efferocytosis, infectious disease, and cancer. Cell Death Differ. 23, 962–978 (2016).
16. Deigner, H.P.; Hermetter, A. Oxidized phospholipids: Emerging lipid mediators in pathophysiology. Curr. Opin. Lipidol. 19, 289–294 (2008).
17. Cheng, M.; Bhujwalla, Z.M.; Glunde, K. Targeting phospholipid metabolism in cancer. Front. Oncol. 6, 266 (2016).
18. Ashraf, M.Z.; Kar, N.S.; Podrez, E.A. Oxidized phospholipids: Biomarker for cardiovascular diseases. Int. J. Biochem. Cell Biol. 41, 1241–1244 (2009).
19. Chang, W.; Hatch, G.M.; Wang, Y.; Yu, F.; Wang, M. The relationship between phospholipids and insulin resistance: From clinical to experimental studies. J. Cell. Mol. Med. 23, 702–710 (2019).
20. Kosicek, M.; Hecimovic, S. Phospholipids and Alzheimer's disease: Alterations, mechanisms and potential biomarkers. Int. J. Mol. Sci. 14, 1310–1322(2013).
21. Kao, Y.-C.; Ho, P.-C.; Tu, Y.-K.; Jou, I.-M.; Tsai, K.-J. Lipids and Alzheimer's Disease. Int. J. Mol. Sci. 21, 1505(2020).
22. Cas, M.D.; Roda, G.; Li, F.; Secundo, F. Functional lipids in autoimmune inflammatory diseases. Int. J. Mol. Sci. 21(2020).
23. van Goor, H.; Gerrits, P.O.; Grond, J. The application of lipid-soluble stains in plastic-embedded sections. Histochemistry. 85, 251–253 (1986).
24. Mehlem, A.; Hagberg, C.E.; Muhl, L.; Eriksson, U.; Falkevall, A. Imaging of neutral lipids by oil red O for analyzing the metabolic status in health and disease. Nat. Protoc. 8, 1149–1154 (2013).
25. Fowler, S.D.; Greenspan, P. Application of Nile red, a fluorescent hydrophobic probe, for the detection of neutral lipid deposits in tissue sections: Comparison with oil red O. J. Histochem. Cytochem. 33, 833–836(1985).
26. Wigglesworth, V.B. Histological staining of lipids for the light and electron microscope. Biol. Rev. Camb. Philos. Soc. 63, 417–431(1988).
27. Cajka, T.; Fiehn, O. Comprehensive analysis of lipids in biological systems by liquid chromatography-mass spectrometry. TrAC - Trends Anal. Chem. 61, 192–206(2014).
28. Long, N.P.; Park, S.; Anh, N.H.; et al. Advances in Liquid Chromatography–Mass Spectrometry-Based Lipidomics: A Look Ahead. J. Anal. Test. 4, 183–197(2020).
29. Berkecz, R.; Tömösi, F.; Körmöczi, T.; Szegedi, V.; Horváth, J.; Janáky, T. Comprehensive phospholipid and sphingomyelin profiling of different brain regions in mouse model of anxiety disorder using online two-dimensional (HILIC/RP)-LC/MS method. J. Pharm. Biomed. Anal. 149, 308–317(2018).
30. Lin, Y.; Gu, H.; Jiang, L.; et al. Cocaine modifies brain lipidome in mice. Mol. Cell. Neurosci. 85, 29–44(2017).
31. Zimmerman, T.A.; Monroe, E.B.; Tucker, K.R.; Rubakhin, S.S.; Sweedler, J. V. Imaging of cells and tissues with mass spectrometry. adding chemical information to imaging. Methods Cell Biol. 89, 361–390(2008).
32. Buchberger, A.R.; DeLaney, K.; Johnson, J.; Li, L. Mass spectrometry imaging: a review of emerging advancements and future insights. Anal. Chem. 90, 240–265(2018).
33. Fahy, E.; Subramaniam, S.; Brown, H.A.; et al. A comprehensive classification system for lipids. J. Lipid Res. 46, 839–861(2005).

34. Saito, Y.; Waki, M.; Hameed, S.; Hayasaka, T.; Setou, M. Development of imaging mass spectrometry. Biol. Pharm. Bull. 35, 1417–1424(2012).
35. Caprioli, R.M.; Farmer, T.B.; Gile, J. Molecular Imaging of Biological Samples: Localization of Peptides and Proteins Using MALDI-TOF MS. Anal. Chem. 69, 4751–4760(1997).
36. Goto-Inoue, N.; Hayasaka, T.; Zaima, N.; Setou, M. Imaging mass spectrometry for lipidomics. Biochim. Biophys. Acta - Mol. Cell Biol. Lipids. 1811, 961–969(2011).
37. Eriksson, C.; Masaki, N.; Yao, I.; Hayasaka, T.; Setou, M. MALDI imaging mass spectrometry—a mini review of methods and recent developments. Mass Spectrom. 2, S0022–S0022(2013).
38. Wiseman, J.M.; Ifa, D.R.; Song, Q.; Cooks, R.G. Tissue imaging at atmospheric pressure using desorption electrospray ionization (DESI) mass spectrometry. Angew. Chemie Int. Ed. 45, 7188–7192(2006).
39. Anderton, C.R.; Gamble, L.J. Secondary ion mass spectrometry imaging of tissues, cells, and microbial systems. Micros. Today. 24, 24–31(2016).
40. Bokhart, M.T.; Muddiman, D.C. Infrared matrix-assisted laser desorption electrospray ionization mass spectrometry imaging analysis of biospecimens. Analyst. 141, 5236–5245(2016).
41. Robichaud, G.; Barry, J.A.; Garrard, K.P.; Muddiman, D.C. Infrared matrix-assisted laser desorption electrospray ionization (IR-MALDESI) imaging source coupled to a FT-ICR mass spectrometer. J. Am. Soc. Mass Spectrom. 24, 92–100(2013).
42. Schaepe, K.; Bhandari, D.R.; Werner, J.; et al. Imaging of lipids in native human bone sections using TOF-secondary ion mass spectrometry, atmospheric pressure scanning microprobe matrix-assisted laser desorption/ionization orbitrap mass spectrometry, and orbitrap-secondary ion mass spectrometry. Anal. Chem. 90, 8856–8864(2018).
43. Kompauer, M.; Heiles, S.; Spengler, B. Atmospheric pressure MALDI mass spectrometry imaging of tissues and cells at 1.4-μm lateral resolution. Nat. Methods. 14, 90–96(2016).
44. Tata, A.; Fernandes, A.M.A.P.; Santos, V.G.; Alberici, R.M.; Araldi, D.; Parada, C.A.; Braguini, W.; Veronez, L.; Silva Bisson, G.; Reis, F.H.Z.; et al. Nanoassisted laser desorption-ionization-MS imaging of tumors. Anal. Chem. 2012, 84, 6341–6345(2012).
45. Kuwata, K.; Itou, K.; Kotani, M.; Ohmura, T.; Naito, Y. DIUTHAME enables matrix‐free mass spectrometry imaging of frozen tissue sections. Rapid Commun. Mass Spectrom. 34(2020).
46. Nemes, P.; Woods, A.S.; Vertes, A. Simultaneous imaging of small metabolites and lipids in rat brain tissues at atmospheric pressure by laser ablation electrospray ionization mass spectrometry. Anal. Chem. 82, 982–988(2010).
47. Luo, Z.; He, J.; Chen, Y.; et al. Air flow-assisted ionization imaging mass spectrometry method for easy whole-body molecular imaging under ambient conditions. Anal. Chem. 85, 2977–2982(2013).
48. Alberici, R.M.; Vendramini, P.H.; Eberlin, M.N. Easy ambient sonic-spray ionization mass spectrometry for tissue imaging. Anal. Methods. 9, 5029–5036(2017).

721 49. Sugiura, Y.; Shimma, S.; Setou, M. Thin sectioning improves the peak intensity
722 and signal-to-noise ratio in direct tissue mass spectrometry. J. Mass Spectrom.
723 Soc. Jpn. 54, 45–48(2006).
724 50. Leopold, J.; Popkova, Y.; Engel, K.M.; Schiller, J. Recent developments of useful
725 MALDI matrices for the mass spectrometric characterization of lipids.
726 Biomolecules. 8(2018).
727 51. Wang, H.Y.J.; Post, S.N.J.J.; Woods, A.S. A minimalist approach to MALDI
728 imaging of glycerophospholipids and sphingolipids in rat brain sections. Int. J.
729 Mass Spectrom. 278, 143–149(2008).
730 52. Vermillion-Salsbury, R.L.; Hercules, D.M. 9-Aminoacridine as a matrix for
731 negative mode matrix-assisted laser desorption/ionization. Rapid Commun. Mass
732 Spectrom. 16, 1575–1581(2002).
733 53. Hayasaka, T.; Goto-Inoue, N.; Masaki, N.; Ikegami, K.; Setou, M. Application of
734 2,5-dihydroxyacetophenone with sublimation provides efficient ionization of
735 lipid species by atmospheric pressure matrix-assisted laser desorption/ionization
736 imaging mass spectrometry. *Surf. Interface Anal.* **2014**, *46*, 1219–1222(2014).
737 54. Wang, Z.; Cai, Y.; Wang, Y.; Zhou, X.; Zhang, Y.; Lu, H. Improved MALDI
738 imaging MS analysis of phospholipids using graphene oxide as new matrix. Sci.
739 Rep. 7, 1–9(2017).
740 55. Ibrahim, H.; Jurcic, K.; Wang, J.S.H.; Whitehead, S.N.; Yeung, K.K.C. 1,6-
741 Diphenyl-1,3,5-hexatriene (DPH) as a novel matrix for maldi ms imaging of fatty
742 acids, phospholipids, and sulfatides in brain tissues. Anal. Chem. 89, 12828–
743 12836(2017).
744 56. Shimma, S.; Sugiura, Y. Effective sample preparations in imaging mass
745 spectrometry. Mass Spectrom. 3, S0029–S0029(2014).
746 57. Passarelli, M.K.; Winograd, N. Lipid imaging with time-of-flight secondary ion
747 mass spectrometry (ToF-SIMS). Biochim. Biophys. Acta - Mol. Cell Biol. Lipids,
748 1811, 976–990(2011).
749 58. Li, H.W.; Hua, X.; Long, Y.T. Metal/matrix enhanced time-of-flight secondary
750 ion mass spectrometry for single cell lipids analysis. Chinese J. Anal. Chem. 46,
751 61–66(2018).
752 59. Malm, J.; Giannaras, D.; Riehle, M.O.; Gadegaard, N.; Sjövall, P. Fixation and
753 drying protocols for the preparation of cell samples for time-of-flight secondary
754 ion mass spectrometry analysis. Anal. Chem. 81, 7197–7205(2009).
755 60. Imaging Mass Spectrometry; Setou, M., Ed.; Springer Japan: Tokyo, ISBN 978-
756 4-431-09424-1(2010).
757 61. Dreisewerd, K. The desorption process in MALDI. Chem. Rev. 103, 395–
758 425(2003).
759 62. Murray, K.K. Lasers for matrix‐assisted laser desorption ionization. J. Mass
760 Spectrom. (2020).
761 63. Takats, Z.; Wiseman, J.M.; Gologan, B.; Cooks, R.G. Mass spectrometry
762 sampling under ambient conditions with desorption electrospray ionization.
763 Science. 306, 471–473(2004).
764 64. Yin, R.; Burnum-Johnson, K.E.; Sun, X.; Dey, S.K.; Laskin, J. High spatial
765 resolution imaging of biological tissues using nanospray desorption electrospray
766 ionization mass spectrometry. Nat. Protoc.14, 3445–3470(2019).

65. Nguyen, S.N.; Sontag, R.L.; Carson, J.P.; Corley, R.A.; Ansong, C.; Laskin, J. Towards high-resolution tissue imaging using nanospray desorption electrospray ionization mass spectrometry coupled to shear force microscopy. J. Am. Soc. Mass Spectrom. 29, 316–322(2018).
66. Yin, R.; Kyle, J.; Burnum-Johnson, K.; Bloodsworth, K.J.; Sussel, L.; Ansong, C.; Laskin, J. High spatial resolution imaging of mouse pancreatic islets using nanospray desorption electrospray ionization mass spectrometry. Anal. Chem. 90, 6548–6555(2018).
67. Parrot, D.; Papazian, S.; Foil, D.; Tasdemir, D. Imaging the unimaginable: desorption electrospray ionization – imaging mass spectrometry (DESI-IMS) in natural product research. Planta Med. 84, 584–593(2018).
68. Eberlin, L.S.; Ferreira, C.R.; Dill, A.L.; Ifa, D.R.; Cooks, R.G. Desorption electrospray ionization mass spectrometry for lipid characterization and biological tissue imaging. Biochim. Biophys. Acta - Mol. Cell Biol. Lipids. 1811, 946–960(2011).
69. Chandra, S. Challenges of biological sample preparation for SIMS imaging of elements and molecules at subcellular resolution. Appl. Surf. Sci. 255, 1273–1284(2008).
70. Wishart, D.S.; Tzur, D.; Knox, C.; et al. HMDB: The human metabolome database. Nucleic Acids Res. 35(2007).
71. Mullard, A. Finding the way with LIPID MAPS. Nat. Rev. Mol. Cell Biol. 9, 92–92(2008).
72. Islam, A.; Takeyama, E.; Mamun, M. Al; et al. Green nut oil or DHA supplementation restored decreased distribution levels of DHA containing phosphatidylcholines in the brain of a mouse model of dementia. Metabolites. 10(2020).
73. Ide, Y.; Waki, M.; Hayasaka, T.; et al. Human breast cancer tissues contain abundant phosphatidylcholine(36∶1) with high stearoyl-coa desaturase-1 expression. PLoS One. 8, e61204(2013).
74. Uehara, T.; Kikuchi, H.; Miyazaki, S.; et al. Overexpression of lysophosphatidylcholine acyltransferase 1 and concomitant lipid alterations in gastric cancer. Ann. Surg. Oncol. 23, 206–213(2016).
75. Sparvero, L.J.; Amoscato, A.A.; Dixon, C.E.; et al. Mapping of phospholipids by MALDI imaging (MALDI-MSI): Realities and expectations. Chem. Phys. Lipids. 165, 545–562(2012).
76. Sugiura, Y.; Konishi, Y.; Zaima, N.; et al. Visualization of the cell-selective distribution of PUFA-containing phosphatidylcholines in mouse brain by imaging mass spectrometry. J. Lipid Res. 50, 1776−1788(2009).
77. Kobayashi, Y.; Hayasaka, T.; Setou, M.; Itoh, H.; Kanayama, N. Comparison of phospholipid molecular species between terminal and stem villi of human term placenta by imaging mass spectrometry. Placenta. 31, 245–248(2010).
78. Kurabe, N.; Igarashi, H.; Ohnishi, I.; et al. Visualization of sphingolipids and phospholipids in the fundic gland mucosa of human stomach using imaging mass spectrometry. World J. Gastrointest. Pathophysiol. 7, 235(2016).
79. Ellis, S.R.; Wu, C.; Deeley, J.M.; et al. Imaging of human lens lipids by desorption electrospray ionization mass spectrometry. J. Am. Soc. Mass Spectrom. 21, 2095–2104(2010).

80. Carter, C.L.; McLeod, C.W.; Bunch, J. Imaging of phospholipids in formalin fixed rat brain sections by matrix assisted laser desorption/ionization mass spectrometry. J. Am. Soc. Mass Spectrom. 22, 1991–1998(2011).
81. Jackson, S.N.; Ugarov, M.; Egan, T.; et al. MALDI-ion mohility-TOFMS imaging of lipids in rat brain tissue. J. Mass Spectrom. 42, 1093–1098(2007).
82. Cerruti, C.D.; Benabdellah, F.; Laprévote, O.; Touboul, D.; Brunelle, A. MALDI imaging and structural analysis of rat brain lipid negative ions with 9-aminoacridine matrix. Anal. Chem. 84, 2164–2171(2012).
83. Jackson, S.N.; Baldwin, K.; Muller, L.; et al. Imaging of lipids in rat heart by MALDI-MS with silver nanoparticles. Anal. Bioanal. Chem. 406, 1377–1386(2014).
84. Flinders, B.; Huizing, L.R.S.; Van Heerden, M.; et al. Cross-Species Molecular Imaging of Bile Salts and Lipids in Liver: Identification of Molecular Structural Markers in Health and Disease. Anal. Chem. 90, 11835–11846(2018).
85. Murphy, R.C.; Hankin, J.A.; Barkley, R.M. Imaging of lipid species by MALDI mass spectrometry. (2009).
86. Berry, K.A.Z.; Li, B.; Reynolds, S.D.; et al. MALDI imaging MS of phospholipids in the mouse lung. J. Lipid Res. 52, 1551–1560(2011).
87. Seng, J.; Nealon, J.; Blanksby, S.; Mitchell, T. Distribution of glycerophospholipids in the adult human lens. Biomolecules. 8, 156(2018).
88. Sjövall, P.; Lausmaa, J.; Johansson, B. Mass spectrometric imaging of lipids in brain tissue. Anal. Chem. 76, 4271–4278(2004).
89. Touboul, D.; Brunelle, A. TOF-SIMS imaging of lipids on rat brain sections. Methods Mol. Biol. 1203, 21–27(2015).
90. Magnusson, Y.; Friberg, P.; Sjövall, P.; Dangardt, F.; Malmberg, P.; Chen, Y. Lipid imaging of human skeletal muscle using TOF-SIMS with bismuth cluster ion as a primary ion source. Clin. Physiol. Funct. Imaging. 28, 202–209(2008).
91. Hameed, S.; Ikegami, K.; Sugiyama, E.; et al. Direct profiling of the phospholipid composition of adult Caenorhabditis elegans using whole-body imaging mass spectrometry. Anal. Bioanal. Chem. 407, 7589–7602(2015).
92. Niehoff, A.C.; Kettling, H.; Pirkl, A.; Chiang, Y.N.; Dreisewerd, K.; Yew, J.Y. Analysis of drosophila lipids by matrix-assisted laser desorption/ionization mass spectrometric imaging. Anal. Chem. 86, 11086–11092(2014).
93. Sans, M.; Gharpure, K.; Tibshirani, R.; et al. Metabolic markers and statistical prediction of serous ovarian cancer aggressiveness by ambient ionization mass spectrometry imaging. Cancer Res. 77, 2903–2913(2017).
94. Masterson, T.A.; Dill, A.L.; Eberlin, L.S.; et al. Distinctive glycerophospholipid profiles of human seminoma and adjacent normal tissues by desorption electrospray ionization imaging mass spectrometry. J. Am. Soc. Mass Spectrom. 22, 1326–1333(2011).
95. Margulis, K.; Chiou, A.S.; Aasi, S.Z.; Tibshirani, R.J.; Tang, J.Y.; Zare, R.N. Distinguishing malignant from benign microscopic skin lesions using desorption electrospray ionization mass spectrometry imaging. Proc. Natl. Acad. Sci. U. S. A. 115, 6347–6352(2018).
96. Morita, Y.; Sakaguchi, T.; Ikegami, K.; et al. Lysophosphatidylcholine acyltransferase 1 altered phospholipid composition and regulated hepatoma progression. J. Hepatol. 59, 292–299(2013).

97. Ikedo, T.; Minami, M.; Kataoka, H.; et al. Imaging mass spectroscopy delineates the thinned and thickened walls of intracranial aneurysms. Biochem. Biophys. Res. Commun. 495, 332–338(2018).
98. Koizumi, S.; Yamamoto, S.; Hayasaka, T.; et al. Imaging mass spectrometry revealed the production of lyso-phosphatidylcholine in the injured ischemic rat brain. Neuroscience. 168, 219–225(2010).
99. Mihara, Y.; Horikawa, M.; Sato, S.; et al. Lysophosphatidic acid precursor levels decrease and an arachidonic acid-containing phosphatidylcholine level increases in the dorsal root ganglion of mice after peripheral nerve injury. Neurosci. Lett. 698, 69–75(2019).
100. Aoki, J.; Taira, A.; Takanezawa, Y.; et al. Serum lysophosphatidic acid is produced through diverse phospholipase pathways. J. Biol. Chem. 277, 48737–48744(2002).
101. Yuki, D.; Sugiura, Y.; Zaima, N.; et al. DHA-PC and PSD-95 decrease after loss of synaptophysin and before neuronal loss in patients with Alzheimer's disease. Sci. Rep. 4(2014).
102. Takeyama, E.; Islam, A.; Watanabe, N.; et al. Dietary intake of green nut oil or DHA ameliorates DHA distribution in the brain of a mouse model of dementia accompanied by memory recovery. Nutrients. 11(2019).
103. Philipsen, M.H.; Phan, N.T.N.; Fletcher, J.S.; Malmberg, P.; Ewing, A.G. Mass spectrometry imaging shows cocaine and methylphenidate have opposite effects on major lipids in drosophila brain. ACS Chem. Neurosci. 9, 1462–1468(2018).
104. Kurabe, N.; Hayasaka, T.; Ogawa, M.; et al. Accumulated phosphatidylcholine (16:0/16:1) in human colorectal cancer; possible involvement of LPCAT4. Cancer Sci. 104, 1295–1302(2013).
105. Hosokawa, Y.; Masaki, N.; Takei, S.; et al. Recurrent triple-negative breast cancer (TNBC) tissues contain a higher amount of phosphatidylcholine (32:1) than non-recurrent TNBC tissues. PLoS One. 12, e0183724(2017).
106. Goto, T.; Terada, N.; Inoue, T.; et al. Decreased expression of lysophosphatidylcholine (16:0/OH) in high resolution imaging mass spectrometry independently predicts biochemical recurrence after surgical treatment for prostate cancer. Prostate. 75, 1821–1830(2015).
107. Dill, A.L.; Eberlin, L.S.; Costa, A.B.; et al. Multivariate statistical identification of human bladder carcinomas using ambient ionization imaging mass spectrometry. Chem. - A Eur. J. 17, 2897–2902(2011).
108. Eberlin, L.S.; Norton, I.; Dill, A.L.; et al. Classifying human brain tumors by lipid imaging with mass spectrometry. Cancer Res. 72, 645–654(2012).
109. Dill, A.L.; Eberlin, L.S.; Zheng, C.; et al. Multivariate statistical differentiation of renal cell carcinomas based on lipidomic analysis by ambient ionization imaging mass spectrometry. Anal. Bioanal. Chem. 398, 2969–2978(2010).
110. Guenther, S.; Muirhead, L.J.; Speller, A.V.M.; et al. Spatially resolved metabolic phenotyping of breast cancer by desorption electrospray ionization mass spectrometry. Cancer Res. 75, 1828–1837(2015).
111. Mao, X.; He, J.; Li, T.; et al. Application of imaging mass spectrometry for the molecular diagnosis of human breast tumors. Sci. Rep. 6, 1–12(2016).

112. Stubbs, C.D.; Smith, A.D. The modification of mammalian membrane polyunsaturated fatty acid composition in relation to membrane fluidity and function. BBA - Rev. Biomembr. 779, 89–137(1984).
113. Ishikawa, S.; Tateya, I.; Hayasaka, T.; et al. The distribution of phosphatidylcholine species in superficial-type pharyngeal carcinoma. Biomed Res. Int. (2017).
114. Kiebish, M.A.; Han, X.; Cheng, H.; Chuang, J.H.; Seyfried, T.N. Cardiolipin and electron transport chain abnormalities in mouse brain tumor mitochondria: Lipidomic evidence supporting the Warburg theory of cancer. J. Lipid Res. 49, 2545–2556(2008).
115. Hayasaka, T.; Fuda, H.; Hui, S.-P.; Chiba, H. Imaging mass spectrometry reveals a decrease of cardiolipin in the kidney of NASH model mice. Anal. Sci. 32, 473–476(2016).
116. Amoscato, A.A.; Sparvero, L.J.; He, R.R.; Watkins, S.; Bayir, H.; Kagan, V.E. Imaging mass spectrometry of diversified cardiolipin molecular species in the brain. Anal. Chem. 86, 6587–6595(2014).
117. Sparvero, L.J.; Amoscato, A.A.; Fink, A.B.; et al. Imaging mass spectrometry reveals loss of polyunsaturated cardiolipins in the cortical contusion, hippocampus, and thalamus after traumatic brain injury. J. Neurochem. 139, 659–675(2016).
118. Yang, H.; Jackson, S.N.; Woods, A.S.; Goodlett, D.R.; Ernst, R.K.; Scott, A.J. Streamlined analysis of cardiolipins in prokaryotic and eukaryotic samples using a norharmane matrix by MALDI-MSI. J. Am. Soc. Mass Spectrom. 31, 2495–2502(2020).
119. Eberlin, L.S.; Gabay, M.; Fan, A.C.; et al. Alteration of the lipid profile in lymphomas induced by MYC overexpression. Proc. Natl. Acad. Sci. U. S. A. 111, 10450–10455(2014).
120. Zhang, J.; Yu, W.; Ryu, S.W.; et al. Cardiolipins are biomarkers of mitochondria-rich thyroid oncocytic tumors. Cancer Res. 76, 6588–6597(2016).
121. Spickett, C.M.; Pitt, A.R. Oxidative lipidomics coming of age: Advances in analysis of oxidized phospholipids in physiology and pathology. Antioxidants Redox Signal. 22, 1646–1666(2015).
122. Li, L.; Zhong, S.; Shen, X.; et al. Recent development on liquid chromatography-mass spectrometry analysis of oxidized lipids. Free Radic. Biol. Med. 144, 16–34(2019).
123. Hossen, M.A.; Nagata, Y.; Waki, M.; et al. Decreased level of phosphatidylcholine (16:0/20:4) in multiple myeloma cells compared to plasma cells: a single-cell MALDI–IMS approach. Anal. Bioanal. Chem. 407, 5273–5280(2015).
124. Schober, Y.; Guenther, S.; Spengler, B.; Römpp, A. Single cell matrix-assisted laser desorption/ionization mass spectrometry imaging. Anal. Chem. 84, 6293–6297(2012).
125. Ostrowski, S.G.; Van Bell, C.T.; Winograd, N.; Ewing, A.G. Mass spectrometric imaging of highly curved membranes during Tetrahymena mating. Science. 305, 71–73(2004).

126. Patterson, N.H.; Doonan, R.J.; Daskalopoulou, S.S.; et al. Three-dimensional imaging MS of lipids in atherosclerotic plaques: Open-source methods for reconstruction and analysis. Proteomics. 16, 1642–1651(2016).
127. Dueñas, M.E.; Essner, J.J.; Lee, Y.J. 3D MALDI mass spectrometry imaging of a single cell: spatial mapping of lipids in the embryonic development of Zebrafish. Sci. Rep. 7(2017).
128. Paine, M.R.L.; Liu, J.; Huang, D.; et al. Three-dimensional mass spectrometry imaging identifies lipid markers of medulloblastoma metastasis. Sci. Rep. 9(2019).
129. Eberlin, L.S.; Ifa, D.R.; Wu, C.; Cooks, R.G. Three-dimensional vizualization of mouse brain by lipid analysis using ambient ionization mass spectrometry. Angew. Chemie. 122, 885–888(2010).
130. Henderson, F.; Jones, E.; Denbigh, J.; et al. 3D DESI-MS lipid imaging in a xenograft model of glioblastoma: a proof of principle. Sci. Rep. 10(2020).
131. Castellanos, A.; Ramirez, C.E.; Michalkova, V.; Nouzova, M.; Noriega, F.G.; Fernández-Lima, F. Three dimensional secondary ion mass spectrometry imaging (3D-SIMS) of: Aedes aegypti ovarian follicles. J. Anal. At. Spectrom. 34, 874–883(2019).
132. Angel, P.M.; Baldwin, H.S.; Gottlieb Sen, D.; et al. Advances in MALDI imaging mass spectrometry of proteins in cardiac tissue, including the heart valve. Biochim. Biophys. Acta - Proteins Proteomics. 1865, 927–935(2017).
133. Nakashima, Y.; Setou, M. Distribution of antisense oligonucleotides in rat eyeballs using maldi imaging mass spectrometry. Mass Spectrom. 7, A0070–A0070(2018).
134. Eto, F.; Sato, S.; Setou, M.; Yao, I. Region-specific effects of Scrapper on the abundance of glutamate and gamma-aminobutyric acid in the mouse brain. Sci. Rep. 10, 1–10(2020).
135. Shrivas, K.; Hayasaka, T.; Sugiura, Y.; Setou, M. Method for simultaneous imaging of endogenous low molecular weight metabolites in mouse brain using TiO2 nanoparticles in nanoparticle-assisted laser desorption/ionization-imaging mass spectrometry. Anal. Chem. 83, 7283–7289(2011).
136. Sugiura, Y.; Setou, M. Imaging mass spectrometry for visualization of drug and endogenous metabolite distribution: Toward in situ pharmacometabolomes. J. Neuroimmune Pharmacol. 5, 31–43(2010).
137. Sugiura, Y.; Shimma, S.; Setou, M. Two-step matrix application technique to improve ionization efficiency for matrix-assisted laser desorption/ionization in imaging mass spectrometry. Anal. Chem. 78, 8227–8235(2006).
138. Taira, S.; Sugiura, Y.; Moritake, S.; Shimma, S.; Ichiyanagi, Y.; Setou, M. Nanoparticle-assisted laser desorption/ionization based mass imaging with cellular resolution. Anal. Chem. 80, 4761–4766(2008).
139. Mamun, M. Al; Sato, S.; Naru, E.; et al. Higher Accumulation of Docosahexaenoic Acid in the Vermilion of the Human Lip than in the Skin. Int. J. Mol. Sci. 21, 2807(2020).
140. Mamun, M. Al; Gonzalez, T.V.; Islam, A.; et al. Analysis of potential anti-aging beverage Pru, a traditional Cuban refreshment, by desorption electrospray

ionization-mass spectrometry and FTICR tandem mass spectrometry. J. Food Drug Anal. 27(4), 833-840(2019).
141. Sato, T.; Horikawa, M.; Takei, S.; et al. Preferential incorporation of administered eicosapentaenoic acid into thin-cap atherosclerotic plaques. Arterioscler. Thromb. Vasc. Biol. 39, 1802–1816(2019).